Flame folding and conditioned concentration profiles in moderately intense turbulence

Citation for the original published paper (version of record):

Lipatnikov, A., Sabelnikov, V. (2022). Flame folding and conditioned concentration profiles in moderately intense turbulence. Physics of Fluids, 34(6). http://dx.doi.org/10.1063/5.0095866

(article starts on next page)

Flame folding and conditioned concentration profiles in moderately intense turbulence

Andrei N. Lipatnikov[a,*], Vladimir A. Sabelnikov[b]

[a]Department of Mechanics and Maritime Sciences, Chalmers University of Technology, Gothenburg SE-412 96, Sweden
[b]ONERA – The French Aerospace Laboratory, F-91761 Palaiseau, France
*Corresponding author, lipatn@chalmers.se

Abstract

While the flamelet paradigm offers the opportunity to simplify computations of mean species concentrations in turbulent flames, a widely accepted criterion of the validity of this paradigm has not yet been elaborated. In this regard, different physical mechanisms are discussed, and flame folding is one of them. The present work aims at exploring the eventual influence of flame folding on the local flame structure in a turbulent flow. For this purpose, a new diagnostic technique was applied to processing complex-chemistry direct numerical simulation data obtained earlier from a lean hydrogen-air turbulent flame [H.L. Dave and S. Chaudhuri, J. Fluid Mech. 884, A46 (2020)]. The technique consists of counting crossing numbers N_f for a cold boundary of the local reaction zone and a ray normal to the mean flame brush, followed by analyzing statistics sampled from rays characterized by $N_f \geq 3$. More specifically, profiles of species mole fractions, temperature, heat release rate, and species production rates, conditioned to combustion progress variable and either N_f or axial distance Δx between two neighboring reaction zones, are sampled and compared with the counterpart profiles obtained from the laminar flame. Results show that these doubly conditioned profiles are close to each other for various crossing numbers or for various axial distances even if the distance is as small as half laminar flame thickness. The lack of a substantial effect of the crossing number or the axial distance on the doubly conditioned profiles implies that small-scale flame folding does not limit the validity of the flamelet paradigm.

Keywords: Turbulent combustion; Flame folding; Conditioned profiles; Hydrogen

I. ITRODUCTION

Until recently, the focus research into premixed turbulent combustion was placed on the influence of turbulence on a burning rate[1-5] and the influence of a flame on turbulence.[6-10] Currently, due to the threat of global warming, new challenges arise. In particular, an urgent need for development of ultra clean burning technologies calls for efficient methods capable for predicting emissions from combustion engines. From this perspective, the flamelet paradigm[11] is very attractive, because it offers the opportunity to significantly simplify computations of mean concentrations of various species in flames. Initially, this paradigm was developed for modeling weakly turbulent combustion. Recent experimental and numerical studies reviewed by Driscoll et al.,[12] as well as the latest measurements[13] and simulations,[14-25] indicate that premixed flames locally retain the scalar structure of laminar flames even in intense turbulence. In particular, Prof. Pfitzner et al.[21-25] substantially advanced the flamelet approach over the past three years. These recent results extend the domain of applicability of the flamelet paradigm, but boundaries of this domain are still not known.

For instance, flame folding followed by flame-flame interactions is expected to play a more important role with increasing turbulent intensity, thus, reducing predictive capabilities of the flamelet approach in intense turbulence. However, such quite natural expectations should nevertheless be probed. While flame folding and flame-flame interactions were numerically explored in the literature,[25-30] the focus of the earlier studies was placed on turbulent burning rate, flame surface area, or probability density functions. Since these quantities were shown to be substantially affected by flame folding and flame-flame interactions, one could also expect substantial influence of the discussed phenomena on the local scalar structure of the interacting flames. However, the present authors are not aware of research into such an influence. Therefore, a reasonable agreement[12-20] between conditioned profiles of species concentrations or temperature, extracted from highly turbulent flames, with results of simulations of laminar flames could be attributed not only to (i) a minor role played by flame folding and flame-flame interactions under conditions of the cited studies, but also to (ii) statistically weak sensitivity of local flame structure to these phenomena. Even if the latter alternative does not seem to be expected, it should be explored. Since the present authors are not aware of a relevant study, this work aims at filling this knowledge gap by analyzing Direct Numerical Simulation (DNS) data by Dave et al.[31,32].

In the next section, the DNS attributes and data processing methods are reported. Results are discussed in Sect. III, followed by conclusions.

II. DNS ATTRIBUTES AND PROCESSING METHODS

Since the simulations were already discussed in earlier papers,[14,16,31,32] we will restrict ourselves to a brief summary of them. A statistically planar, lean H_2/air flame propagating in a box was simulated using a detailed chemical mechanism (21 reactions, 9 species) by Li et al.[33] jointly with the mixture-averaged molecular transport model. To numerically solve unsteady and three-dimensional compressible continuity, Navier-Stokes, species and energy transport equations in a parallelepiped ($19.18 \times 4.8 \times 4.8$ mm) meshed using a uniform grid of $960 \times 240 \times 240$ cells, the Pencil code[34] was adopted. Navier-Stokes characteristic boundary conditions[35] were set at the inlet and outlet. At the transverse sides, boundary conditions were periodic.

Combustion simulations were started at $t = 0$ by embedding a pre-computed planar laminar flame into the computational domain at $x = x_0$. Subsequently, the flame propagated along the x-axis against a turbulent flow injected into the computational domain through the inlet (left) boundary. Before the start of the combustion simulation, homogeneous isotropic turbulence was generated adopting large-scale forcing in a cube with the fully periodic boundary conditions and was evolved until a statistically stationary state characterized by Kolmogorov-Obukhov's 5/3-spectrum was reached.[31] At $t \geq 0$, this turbulence was injected into the computational domain at a constant mean velocity. The turbulence decayed along the x-axis.

Under the simulation conditions (atmospheric pressure, unburned gas temperature T_u =310 K, and the equivalence ratio $\Phi = 0.81$), the laminar flame speed S_L, thickness $\delta_L =$

$(T_b - T_u)/\max|\nabla T|$, and time scale $\tau_f = \delta_L/S_L$ are equal to 1.84 m/s, 0.36 mm, and 0.20 ms, respectively. The pre-generated homogeneous isotropic turbulence is characterized[32] by the rms velocity $u' = 6.7$ m/s, an integral length scale $L = 3.1$ mm, an integral time scale $\tau_t = L/u' = 0.46$ ms, Kolmogorov length scale $\eta = (\nu_u^3/\langle\varepsilon\rangle)^{1/4} = 0.018$ mm, Kolmogorov time scale $\tau_\eta = (\nu_u/\langle\varepsilon\rangle)^{1/2} = 0.015$ ms, and turbulent Reynolds number $Re_t = u'L/\nu_u = 950$. Thus, Karlovitz number and $Ka = (\delta_L/\eta)^2 = 400$ and Damköhler number $Da = \tau_t/\tau_f = 2.35$. Here, $\langle\varepsilon\rangle = \langle 2\nu S_{ij}S_{ij}\rangle$ is the rate of dissipation of turbulent kinetic energy, averaged over the cube; $S_{ij} = \left(\partial u_i/\partial x_j + \partial u_j/\partial x_i\right)/2$ is the rate-of-strain tensor; ν is the kinematic viscosity of the mixture; the summation convention applies to repeated indexes; subscripts u and b designate unburned and burned gas, respectively. Due to the turbulence decay along the mean flow direction, $u' = 3.3$ m/s at the leading edge of the mean flame brush, whereas the turbulence length scales vary weakly between the inlet boundary and the leading edge.

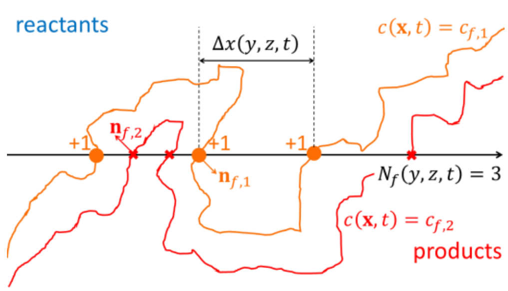

FIG. 1. Diagnostics of flame folding events.

To explore flame folding events and their effects on the local flame structure, the DNS data were processed as follows. First, at each instant t, rays $\{y = y_j, z = z_k\}$ parallel to the x-axis and normal to the mean flame brush were drawn from each grid node in the inlet plane to the outlet plane, see black arrow in Fig. 1. Then, a crossing number N_f was counted for each ray and the cold boundary $c(\mathbf{x},t) = c_{f,1}$ of the reaction zone, see circles on an orange curve in

Fig. 1. Note that if a ray had crossed the cold boundary at least once, the next increase in the crossing number was allowed solely when the ray had also crossed the hot boundary $c(\mathbf{x}, t) = c_{f,2}$ (the latter events shown in crosses on a red curve in Fig. 1 were not counted in N_f). Accordingly, (i) even crossing numbers were associated with local flame elements that move to the right, i.e., to the product side of the flame brush, and (ii) the largest (for each ray) crossing number, i.e., $N_f(y, z, t)$, was an odd number, because $c(y, z, t) > c_{f,2}$ at the outlet.

Results reported in the following were obtained using the temperature-based combustion progress variable $c = (T - T_u)/(T_b - T_u)$. The boundaries $c_{f,1} = 0.10$ and $c_{f,2} = 0.66$ have been set using a constraint of $\dot{\omega}_T\left(c_{f,1}\right) = \dot{\omega}_T\left(c_{f,2}\right) = 0.5\max\{\dot{\omega}_T(c)\}$, where $\dot{\omega}_T(c)$ designates dependence of Heat Release Rate (HRR) on the combustion progress variable in the unperturbed laminar flame. A similar analysis was performed adopting fuel concentration to define another combustion progress variable and setting the reaction zone boundaries for the local Fuel Consumption Rate (FCR) $\dot{\omega}_F(\mathbf{x}, t)$ to be equal to half the peak FCR in the laminar flame. Since major results obtained using (i) the temperature-based combustion progress variable and HRR or (ii) the fuel-based combustion progress variable and FCR are similar, we will restrict ourselves to reporting the former results only.

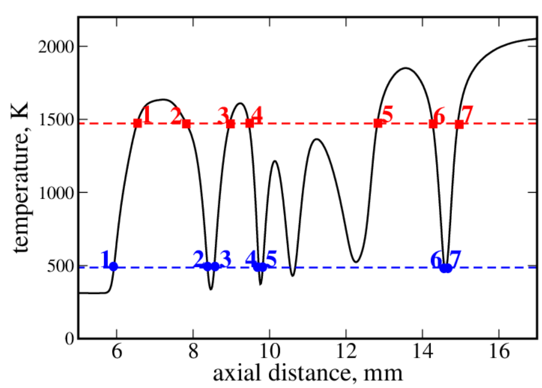

FIG. 2. Typical instantaneous axial temperature profile characterized by the largest obtained $N_f(y, z, t)$. Blue circles and red squares show boundaries of local reaction zones.

Shown in Fig. 2 is a typical instantaneous axial temperature profile characterized by the largest $N_f(y,z,t)=7$ found by processing the DNS data. In some cases, $c_{f,1}=0.10$ and $c_{f,2}=0.66$ bound thick reaction zones, which have complicated local structures, e.g., see the temperature profile between the fifth blue circle and the fifth red square. Such zones appear to be particularly difficult to model using the flamelet approach.

Figure 2 illustrates also that the number $N_f(y,z,t)$ depends on the choice of $c_{f,1}$ and $c_{f,2}$. Indeed, $N_f(y,z,t)=9$ can be obtained by slightly increasing $c_{f,1}$ and decreasing $c_{f,2}$ in order for each shifted horizontal straight dashed line to cross the local dome centered at $x \approx 11.5$ mm twice. Nevertheless, such variations in $c_{f,1}$, $c_{f,2}$, and, hence, $N_f(y,z,t)$ weakly affect doubly conditional profiles discussed below and reported later, because these profiles are almost the same for different $N_f(y,z,t)$, as will be shown in Sect. III.

Doubly conditioned single-point scalar mixture characteristics $\langle \phi | \xi, N_m \rangle$ were sampled from grid points characterized by $\left| c(\mathbf{x},t) - \xi_j \right| < 0.005$ along rays characterized by $N_f(y,z,t)=N_m$ at various instants t. Here, $\xi_j = 0.01j$ with $j=0,\dots,100$ is a sample variable for the instantaneous $c(\mathbf{x},t)$-field and ϕ subsumes mass fraction Y_l of l species, the rate $\dot{\omega}_l$ of its production, temperature T, and HRR. Comparison of the conditional profiles $\langle \phi | \xi, N_m \rangle$ sampled at different N_m offers the opportunity to statistically explore the influence of flame folding on the local flame structure.

Besides, along each ray characterized by $N_f(y,z,t) > 1$, axial distances $\Delta x(y,z,t)$ between two rightmost neighboring crossing points $c(\mathbf{x},t) = c_{f,1}$ (i.e., axial distances between leading edges of two reaction zones that are most close to the outlet boundary, see the distance $\Delta x(y,z,t)$ in Fig. 1 or a small distance between blue circles 6 and 7 in Fig. 2) were calculated. Then, doubly conditioned quantities $\langle \phi | \xi, \Delta_m \rangle$ were sampled along rays characterized by $\Delta_{m-1} < \Delta x(y,z,t) \leq \Delta_m$ and $N_f(y,z,t) > 1$ at all instants. Here, $\Delta_m - \Delta_{m-1} = \delta_L/2$ and $\Delta_0 = 0$. Comparison of the conditional profiles $\langle \phi | \xi, \Delta_m \rangle$ sampled at different Δ_m also offers the opportunity to explore the statistical influence of flame folding on the local flame structure.

The conditional profiles were sampled from 56 snapshots stored, each 5 μs over 1.291 ms $\leq t \leq$1.566 ms or $2.8 \leq t/\tau_t \leq 3.4$).

III. RESULTS AND DISCUSSION

Figure 3 compares evolutions of turbulent burning velocities evaluated by integrating the HRR expressed in g·K/(cm^{3}s) or the flame surface density $\overline{|\nabla c|}(\mathbf{x},t)$ over the computational domain Ω, i.e.,

$$U_t^{HRR}(t) = \frac{1}{\rho_u(T_b - T_u)\Lambda^2} \iiint_\Omega \dot{\omega}_T(\mathbf{x},t)d\mathbf{x}, \tag{1}$$

$$U_t^{FSD}(t) = \frac{S_L}{\Lambda^2} \iiint_\Omega \overline{|\nabla c|}(\mathbf{x},t)d\mathbf{x}. \tag{2}$$

Here, ρ is the density and Λ is the computational domain width. In line with the flamelet paradigm, $U_t^{HRR}(t) \approx U_t^{FSD}(t)$. At the same time, a large $U_t^{HRR}(t) > 5S_L$ implies that flame folding could substantially affect $U_t^{HRR}(t)$.

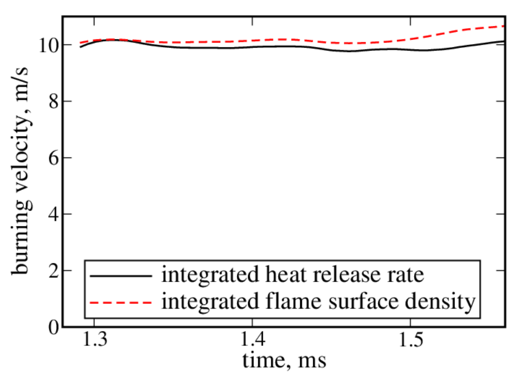

FIG. 3. Evolution of turbulent burning velocities evaluated using Eqs. (1) and (2).

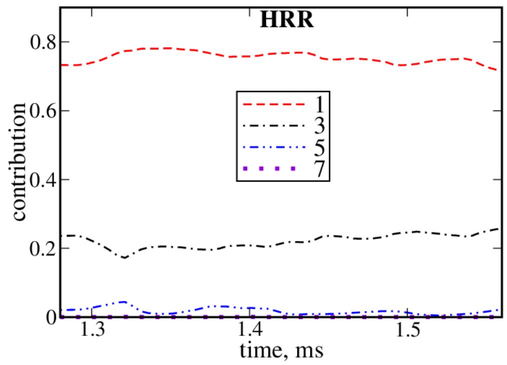

FIG. 4. Contributions of sets of rays, characterized by different $N_f(y,z,t)$ specified in legends, to bulk HRR.

However, Fig. 4 shows that contributions of folded flame elements, i.e., rays characterized by $N_f(y,z,t) \geq 3$, to volume integrated HRR is rather small, always less than 30%. These contributions have been evaluated by integrating the HRR along all rays characterized by the same $N_f(y,z,t) = \mathbb{N}$ and dividing the sum of these integrals with the number $\mathrm{N}_r(\mathbb{N})$ of such rays, i.e.,

$$U_{\mathbb{N}}^{HRR}(t) = \frac{1}{\rho_u(T_b - T_u)\mathrm{N}_r} \sum_{N_f(y,z,t)=\mathbb{N}} \left[\int \dot{\omega}_T(\mathbf{x},t)dx\right]. \quad (3)$$

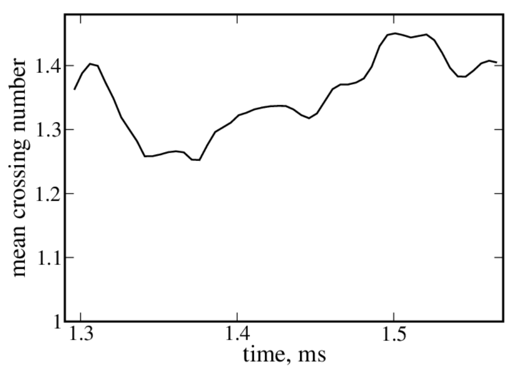

FIG. 5. Evolution of volume-averaged crossing number.

Besides, the mean crossing number $\langle N_f \rangle(t)$, i.e., $N_f(y,z,t)$ averaged over all rays, is also sufficiently small, see Fig. 5, at least, significantly less than $U_t^{HRR}(t)/S_L$. These results are consistent with an earlier DNS study[36] of constant-density highly turbulent reacting waves characterized by various $0.01 \leq Da < 1.0$. That study has shown that an increase in $U_t(t)/S_L$

in a turbulent flow is mainly controlled by inclination of instantaneous flames with respect to the normal to the mean flame brush, whereas flame folding plays a secondary role. The inclination effect is illustrated in Fig. 6, which reports mean values $\langle n_x \rangle(t)$ of $n_x(y, z, t)$ evaluated in all crossing points for the cold (black dotted-dashed line in Fig. 6 and circles in Fig. 1) and hot (red dashed line in Fig. 6 and crosses in Fig. 1) boundaries of reaction zones. Here, n_x is the x-component of the unit normal vector $\mathbf{n} = -\nabla c / |\nabla c|$.

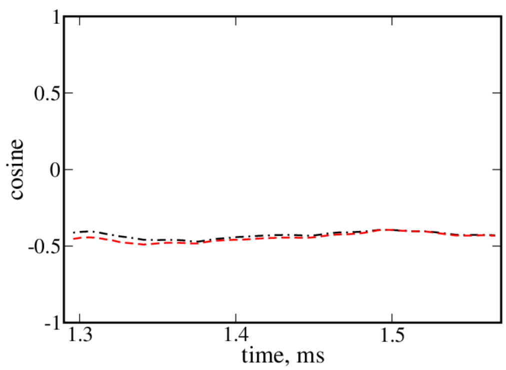

FIG. 6. Volume-averaged cosines $\langle n_x \rangle(t)$ evaluated in all crossing points for the cold (black dotted-dashed line) and hot (red dashed line) boundaries of local reaction zones.

Thus, under conditions of the considered DNS, the probability of folding events is sufficiently low. Accordingly, the capability of flamelet approach for predicting mean mole fractions of various species in the studied flame[14,16] could be attributed to this low probability. However, the probability is sufficiently high (≈20%) to sample statistics conditioned to folding events and to explore the influence of such events on the local flame scalar structure.

Figures 7-9 report the conditional profiles $\langle \phi | \xi, N_m \rangle$ and $\langle \phi | \xi, \Delta_m \rangle$, sampled at different N_m and Δ_m, respectively, for mole fractions ($\phi = X_l$) of H_2, O_2, and H_2O, HRR ($\phi = \dot{\omega}_T$), and rates ($\phi = \dot{\omega}_l$) of consumption of H_2 and O_2 or creation of H_2O. Simple conditioned profiles of $\langle \phi | \xi \rangle$ are not shown, because they were reported earlier[4,6] and are very close to the doubly conditioned profiles for $N_m = 1$ or $\Delta_m = 4\delta_L$. All the conditional profiles, see broken lines, are very close to each other and sufficiently close to the counterpart profiles obtained from the laminar flame, see solid lines. A weak effect of flame folding on the conditional profiles $\langle \phi | \xi, N_m \rangle$ is observed only for $N_m = 7$ and only for HRR or mole fractions of O_2 and H_2O. Moreover, peak absolute values of the considered rates are lower in the laminar flame, but the effect is sufficiently weak.

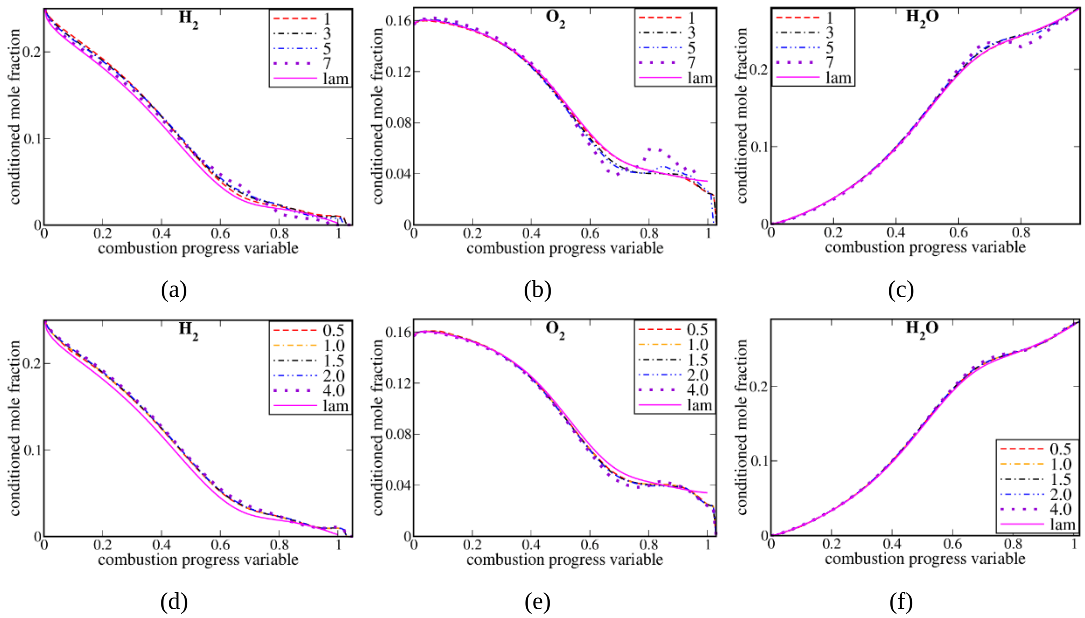

FIG. 7. Mole fractions of (a, d) H_2, (b, e) O_2, and (c, f) H_2O conditioned to combustion progress variable and either (a)-(c) crossing number $N_f(y, z, t)$, i.e., $\langle X_l | \xi, N_m \rangle$, or (d)-(f) distance $\Delta x(y, z, t)$, i.e., $\langle X_l | \xi, \Delta_m \rangle$. Profiles obtained from the laminar flame are plotted in magenta solid lines. Legends in panels (a)-(c) and (d)-(f) report $N_f(y, z, t)$ and Δ_m / δ_L, respectively.

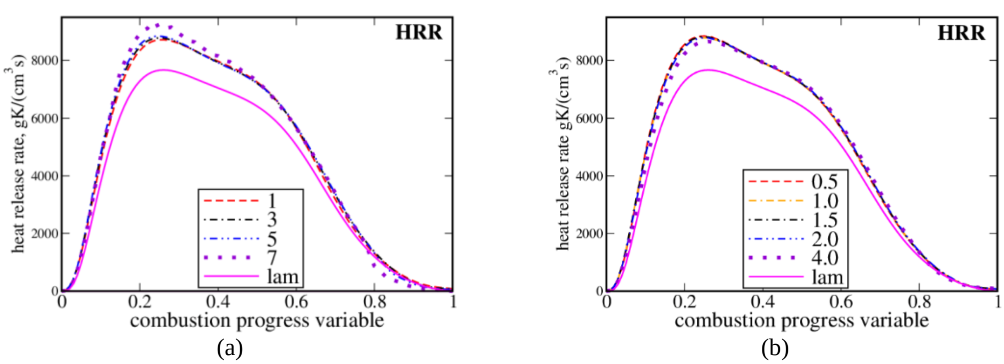

FIG. 8. Heat release rate conditioned to combustion progress variable and either (a) crossing number $N_f(y, z, t)$, i.e., $\langle \dot{\omega}_T | \xi, N_m \rangle$, or (b) distance $\Delta x(y, z, t)$, i.e., $\langle \dot{\omega}_T | \xi, \Delta_m \rangle$. Legends are explained in caption to Fig. 7.

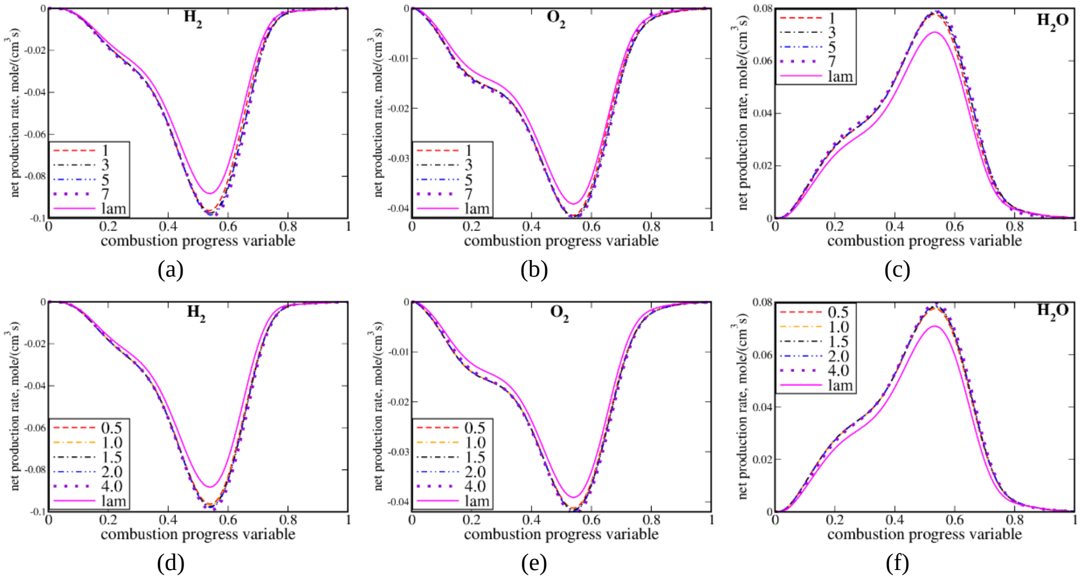

FIG. 9. Production rates for (a, d) H_2, (b, e) O_2, and (c, f) H_2O conditioned to combustion progress variable and either (a)-(c) crossing number $N_f(y,z,t)$ or (d)-(f) distance $\Delta x(y,z,t)$. Legends are explained in caption to Fig. 7.

Figures 10-13 show that the doubly conditioned profiles of radical mole fractions and production rates are also weakly affected by N_m or Δ_m. While differences between the conditional profiles $\langle X_l|\xi, N_m\rangle$ sampled at different N_m and the laminar flame profiles $X_{l,L}(c)$ are increased with N_m for mole fractions of H, O, and OH, see Figs. 10a-10c, these differences are sufficiently small. For mole fractions of HO_2 and H_2O_2 and for all radical production rates, differences between the profiles conditioned to various N_m or Δ_m are significantly less than differences between these profiles and the laminar flame profiles. Accordingly, the validity of the flamelet paradigm is limited by physical mechanisms associated with perturbations of a single local flame (e.g., flame stretching by small-scale turbulent eddies or local variations in the equivalence ratio and temperature due to differential diffusion effects[37]), rather than by flame folding. For instance, due to the differential diffusion effects, the local combustion progress variable can be larger than unity, with differences between the conditional profiles $\langle X_l|\xi, N_m\rangle$ sampled at different N_m and $X_{l,L}(c)$ being most pronounced at $c(\mathbf{x},t) \approx 1$ for O_2, H_2O, OH, and H, see Fig. 7b, 7c, 10b, and 10c.

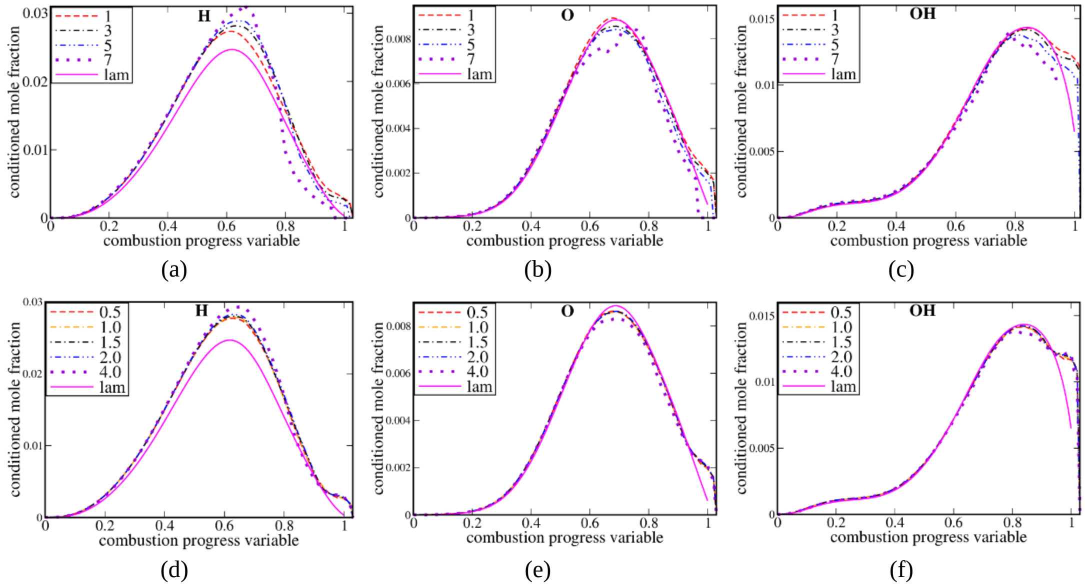

FIG. 10. Mole fractions of the radicals (a, d) H, (b, e) O and (c, f) OH conditioned to combustion progress variable and either (a)-(c) crossing number $N_f(y, z, t)$ or (d)-(f) distance $\Delta x(y, z, t)$. Legends are explained in caption to Fig. 7.

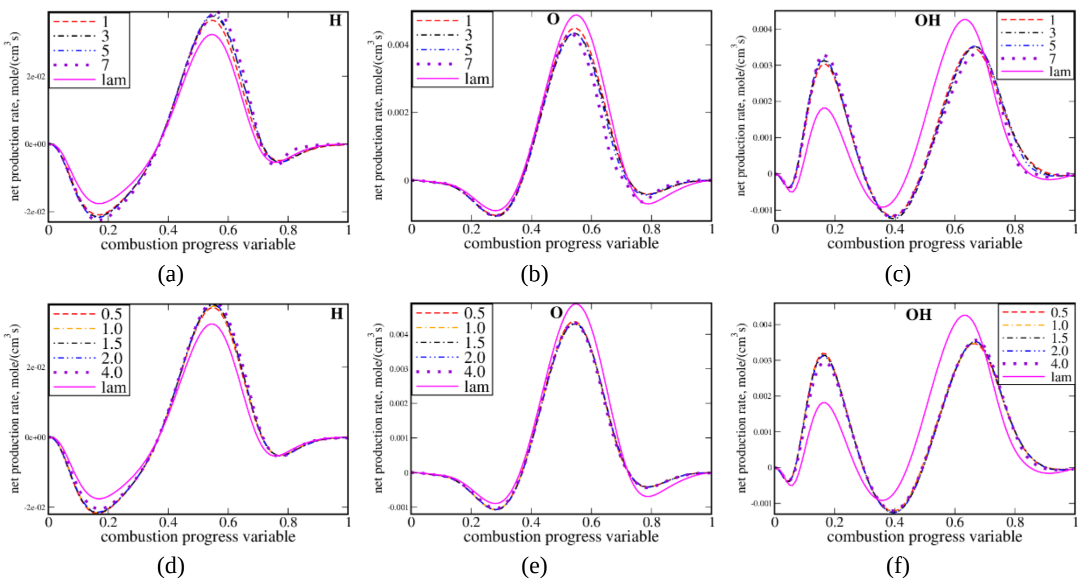

FIG. 11. Rates of production/consumption of the radicals (a, d) H, (b, e) O and (c, f) OH conditioned to combustion progress variable and either (a)-(c) crossing number $N_f(y, z, t)$ or (d)-(f) distance $\Delta x(y, z, t)$. Legends are explained in caption to Fig. 7.

In this regard, it is worth emphasizing the following two points. First, the present work aims mainly at studying the influence of flame holding on the validity of the flamelet paradigm. Therefore, comparison of the conditional profiles $\langle \phi | \xi, N_m \rangle$ sampled at different N_m or the conditional profiles $\langle\phi|\xi,\Delta_m\rangle$ sampled at different Δ_m is of primary interest, whereas the counterpart profiles $\phi_L(c)$ obtained from the unperturbed laminar flame are solely reported for illustration. In other words, investigation of the influence of small-scale turbulent eddies on the simple conditional profiles $\langle\phi|\xi\rangle$ is beyond the scope of the present work. In intense turbulence, variations in $\langle\phi|\xi\rangle$ can stem, e.g., from local strain effects or local intensification of mixing by small-scale turbulent eddies. Within the framework of the flamelet paradigm, such effects could be addressed by invoking the profiles $\phi_L(c)$ obtained from strained laminar flames or equidiffusive laminar flames, e.g., see recent papers by Skiba et al.[13] and Lipatnikov et al.,[18] respectively. Eventual influence of flame folding on the validity of so extended flamelet paradigm should be explored by analyzing DNS data obtained under conditions of sufficiently intense turbulence and this could be a goal for a subsequent study. Under conditions of the DNS analyzed here (moderately intense turbulence), the simplest version of the flamelet paradigm works well. For instance, as discussed in detail elsewhere,[14,16] dependencies of the mean $\bar{\phi}$ on the mean $\bar{c}$ can be well predicted by averaging the profiles $\phi_L(c)$ obtained from the unperturbed laminar flame. Nevertheless, under these conditions, the probability of finding large crossing numbers, i.e., $N_f(y,z,t)=3$, 5, or 7 is sufficiently large, because about $3\cdot10^9$ rays can be sampled from 56 snapshots. Therefore, the conditions of the DNS by Dave et al.[31] fit well to the major goal of the present study, i.e., exploring the influence of flame folding on the conditional profiles $\langle\phi|\xi,N_m\rangle$ sampled at $N_m\geq3$.

Second, while differential diffusion effects are well known[37] to play an important role in lean hydrogen-air flames, the equivalence ratio $\Phi=0.81$ set by Dave et al.[31] is beyond the domain of significant statistical importance of these effects. For instance, in a DNS study by Chen and Im,[38,39] such effects were shown to be weak even at lower $\Phi=0.7$. Statistically significant differential diffusion effects were not revealed in recent analyses[15,17,40] of other

DNS data obtained from lean hydrogen-air flames characterized by $\Phi = 0.7$. Moreover, Fig. 3 shows that turbulent burning velocities evaluated using Eqs. (1) and (2) are very close to one another under the present DNS conditions. Since Eq. (2) involves the unperturbed laminar flame speed S_L, Fig. 3 implies that the influence of differential diffusion phenomena on the local HRR is statistically weak under the studied conditions. Therefore, eventual interaction between flame folding and differential diffusion effects deserves further study by processing DNS data obtained from hydrogen-air flames characterized by a substantially lower equivalence ratio, e.g., $\Phi \leq 0.5$. Nevertheless, local manifestations of differential diffusion effects were documented in the present study, as noted above and below.

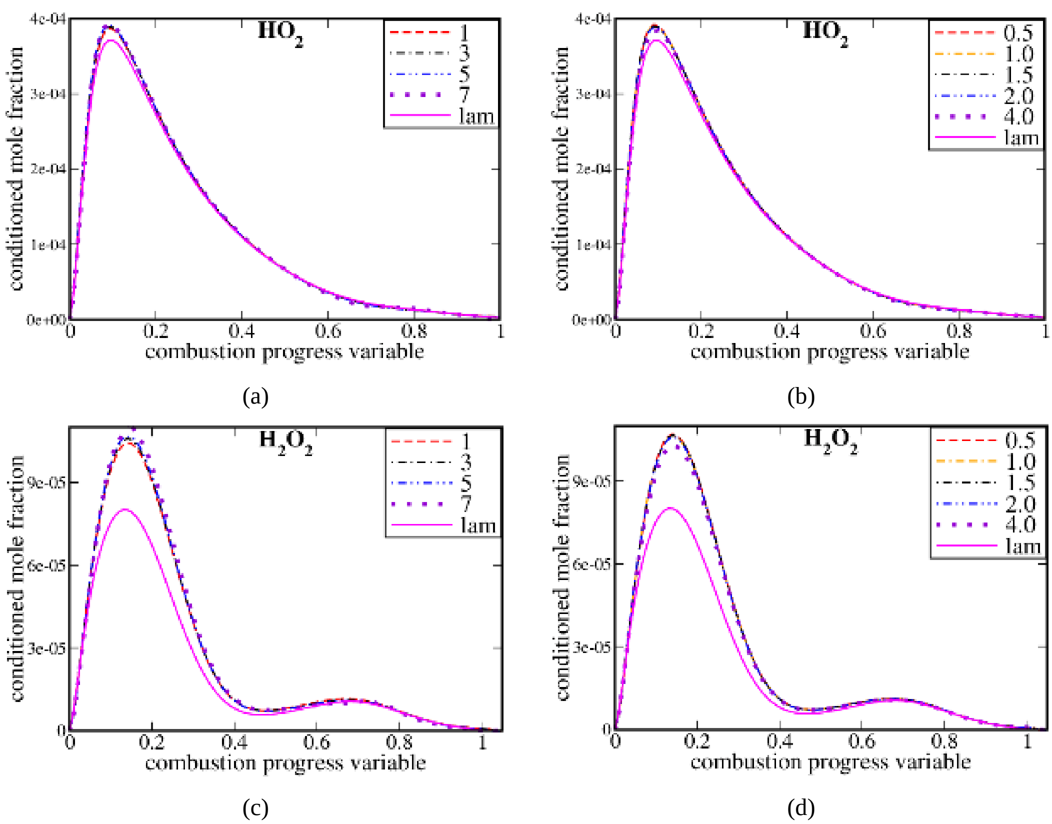

FIG. 12. Mole fractions of (a, b) HO_2 and (c, d) H_2O_2 conditioned to combustion progress variable and either (a, c) crossing number $N_f(y,z,t)$ or (b, d) distance $\Delta x(y,z,t)$. Legends are explained in caption to Fig. 7.

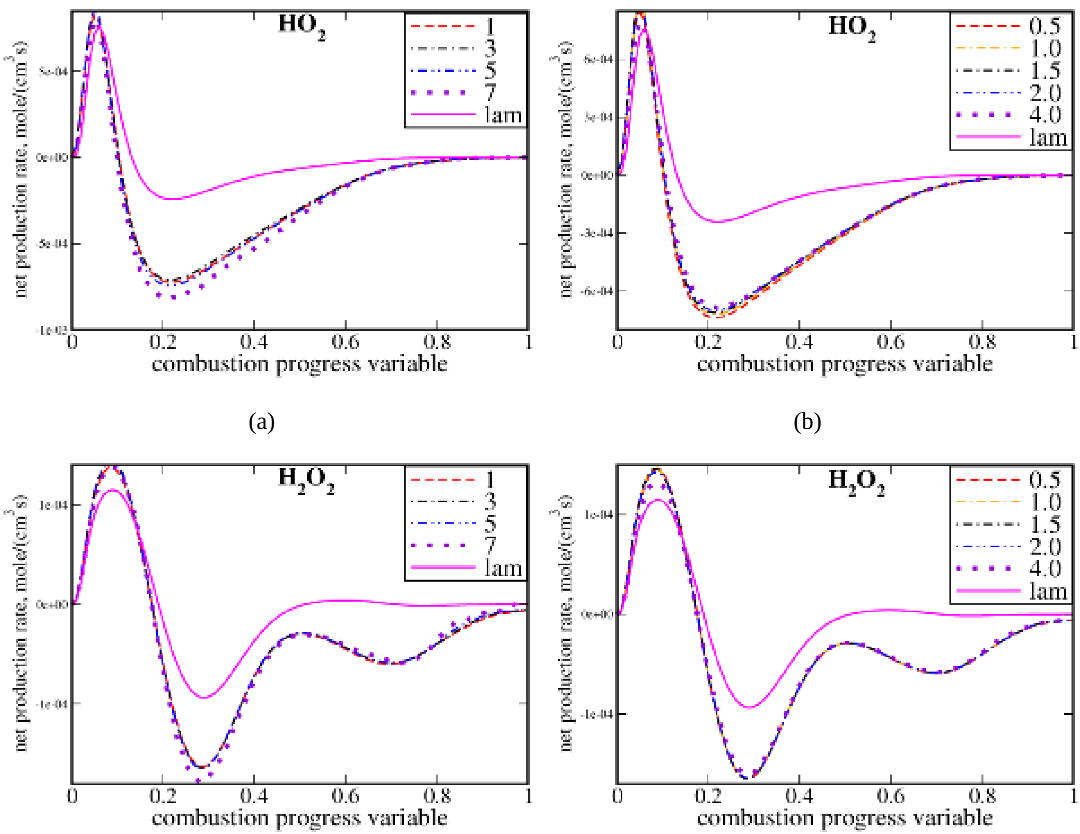

(c) (d)

FIG. 13. Production rates of (a, b) HO_2 and (c, d) H_2O_2 conditioned to combustion progress variable and either (a, c) crossing number $N_f(y,z,t)$ or (b, d) distance $\Delta x(y,z,t)$. Legends are explained in caption to Fig. 7.

While flame folding and flame-flame interactions can result in disappearance of some segments of the interacting flames, the present results imply that surviving flame segments retain their structure to the leading order in the statistical sense. This claim does not mean that instantaneous local differences between $\phi(\mathbf{x},t)$ in a turbulent flame and $\phi[c(\mathbf{x},t)]$ taken from simulations of the counterpart laminar flame are always weak. On the contrary, Fig. 14 shows that such differences can be significant in the vicinity of the local extreme points of the axial profiles sampled from the turbulent flame. Nevertheless, even in this case, the turbulent and laminar flame profiles are close at intermediate values of $c(\mathbf{x},t)$.

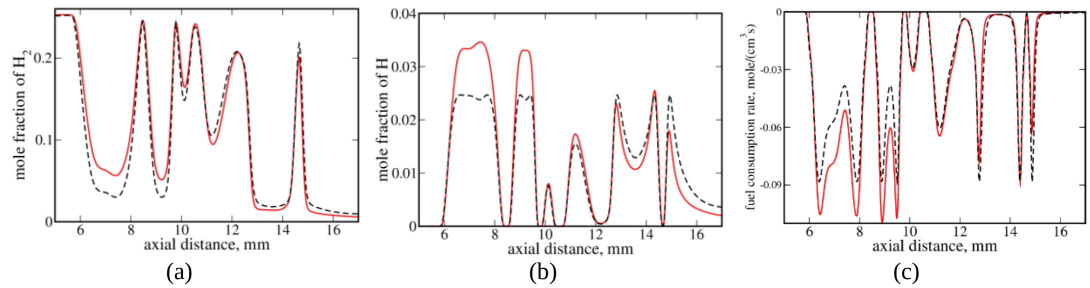

FIG. 14. Instantaneous axial profiles of (a) mole fraction of H_2, (b) mole fraction of H, and (c) fuel production rate, corresponding to the temperature profile plotted in Fig. 2. Red solid lines show profiles sampled from the turbulent flame. Black dashed lines show profiles obtained by substituting $c(x)$ sampled from the turbulent flame into dependencies of $\phi_L(c)$ obtained from the laminar flame.

Figure 14 also indicates that, in the leading zone ($x < 10$ mm) of the flame brush, peak values of $|\phi(x) - \phi_u|$ are larger for the turbulent flame profiles of X_{H_2}, X_{H}, and $\dot{\omega}_{\mathrm{H}_2}$ when compared to the flamelet profiles $\phi_L[c(x)]$, whereas the opposite trend is observed in the trailing zone ($x > 13$ mm). This observation, which typically holds for many other randomly selected axial profiles not reported here for brevity, could be attributed to differential diffusion phenomena. Indeed, for lean hydrogen-air flames, (i) such phenomena are known[37] to result in increasing (decreasing) the local temperature, equivalence ratio, HRR, and fuel consumption rate in positively (negatively, i.e., the curvature center in the unburned reactants) curved reaction zones and (ii) such zones are predominately localized to the leading (trailing) edge of a premixed turbulent flame brush for purely geometrical reasons, e.g., see Fig. 8b in a recent paper by Sabelnikov et al.[40]. Thus, even if differential diffusion phenomena weakly affect (for $\Phi = 0.81$) bulk flame characteristics such as $U_t^{HRR}(t)$, see Fig. 3, such phenomena can play an important role locally.

IV. CONCLUSIONS

To explore eventual influence of flame folding and flame-flame interactions on the structure of local flames in a turbulent flow, new diagnostic techniques were applied to processing DNS data obtained from a moderately turbulent, complex-chemistry, lean hydrogen-air flame. The techniques consist of counting crossing numbers $N_f(y,z,t)$ for a cold boundary of the local reaction zone and a ray normal to the mean flame brush, followed by analyzing statistics sampled from rays characterized by $N_f(y,z,t) \geq 3$. More specifically, profiles of species mole fractions, temperature, heat release rate, and species production rates, conditioned to combustion progress variable and either $N_f(y,z,t)$ or axial distance between two neighboring reaction zones, were sampled and compared.

Results show that the doubly conditioned profiles are close to each other for various crossing numbers or for various axial distances even if the distance is as small as half laminar flame thickness, e.g., see two interacting flames at $x \approx 14.5$ mm in Fig. 2.

The lack of a substantial effect of the crossing number or the axial distance on the doubly conditioned profiles implies that small-scale flame folding is unlikely to limit validity of flamelet paradigm, which seems to be controlled by other physical mechanisms (local flame stretching, differential diffusion, etc.). In the statistical sense, the present results further support using flamelet paradigm for turbulent combustion modeling. Since this study is restricted to analyzing a single moderately turbulent flame, application of the developed diagnostic techniques to other DNS data computed, e.g., at a higher u' or Karlovitz number, appears to be of interest and importance. Nevertheless, certain confidence to the major conclusion regarding weak influence of small-scale flame folding on the flamelet approach validity is given by the facts that (i) the reported profiles have been conditioned to as large as $N_f(y,z,t) = 7$ folding events, (ii) some folding events are associated with a highly perturbed local structure of reaction zones (e.g., see Figs. 2 and 14), but, nevertheless, (iii) the documented influence of variations in $1 \leq N_f(y,z,t) \leq 7$ on the conditioned profiles is very weak.

ACKNOWLEDGEMENTS

The authors are very grateful to Swetaprovo Chaudhuri and Himanshu Dave for providing their DNS data. ANL gratefully acknowledges the financial support provided by Combustion Engine Research Center (CERC). VAS gratefully acknowledges the financial support provided by ONERA.

AUTHOR DECLARATIONS

Conflict of Interest

The authors have no conflicts to disclose.

DATA AVAILABILITY

The data that support the findings of this study are available from the corresponding author upon reasonable request.

REFERENCES

[1] R. Yu and A. N. Lipatnikov, "DNS study of dependence of bulk consumption velocity in a constant-density reacting flow on turbulence and mixture characteristics," Phys. Fluids **29**, 065116 (2017).

[2] L. Cifuentes, C. Dopazo, A. Sandeep, N. Chakraborty, and A. Kempf, "Analysis of flame curvature evolution in a turbulent premixed bluff body burner," Phys. Fluids **30**, 095101 (2018).

[3] A. Y. Klimenko, "The convergence of combustion models and compliance with the Kolmogorov scaling of turbulence," Phys. Fluids **33**, 025112 (2021).

[4] T. Readshaw, T. Ding, S. Rigopoulos, and W. P. Jones, "Modeling of turbulent flames with the large eddy simulation–probability density function (LES–PDF) approach, stochastic fields, and artificial neural networks," Phys. Fluids **33**, 035154 (2021).

[5] V. A. Sabelnikov and A. N. Lipatnikov, "Scaling of reaction progress variable variance in highly turbulent reaction waves," Phys. Fluids **33**, 085103 (2021).

[6] C. Dopazo, L. Cifuentes, and N. Chakraborty, "Vorticity budgets in premixed combusting turbulent flows at different Lewis numbers," Phys. Fluids **29**, 045106 (2017).

[7] A. N. Lipatnikov, V. A. Sabelnikov, S. Nishiki, and T. Hasegawa, "Combustion-induced local shear layers within premixed flamelets in weakly turbulent flows," Phys. Fluids **30**, 085101 (2018).

[8] A. N. Lipatnikov, V. A. Sabelnikov, S. Nishiki, and T. Hasegawa, "Does flame-generated vorticity increase turbulent burning velocity?" Phys. Fluids **30**, 081702 (2018).

[9] P. Brearley, U. Ahmed, N. Chakraborty, and A. N. Lipatnikov, "Statistical behaviours of conditioned two-point second-order structure functions in turbulent premixed flames in different combustion regimes," Phys. Fluids **31**, 115109 (2019).

[10] N. Chakraborty, C. Kasten, U. Ahmed, and M. Klein, "Evolutions of strain rate and dissipation rate of kinetic energy in turbulent premixed flames," Phys. Fluids **33**, 125132 (2021).

[11] N. Peters, *Turbulent Combustion* (Cambridge Univ. Press, Cambridge, UK, 2000).

[12]J. F. Driscoll, J. H. Chen, A. W. Skiba, C. D. Carter, E. R. Hawkes, and H. Wang, "Premixed flames subjected to extreme turbulence: Some questions and recent answers," Prog. Energy Combust. Sci. **76**, 100802 (2020).
[13]A. W. Skiba, C. D. Carter, S. D. Hammack, and J. F. Driscoll, "Experimental assessment of the progress variable space structure of premixed flames subjected to extreme turbulence," Proc. Combust. Inst. **38**, 2893 (2021).
[14]A. N. Lipatnikov and V. A. Sabelnikov, "An extended flamelet-based presumed probability density function for predicting mean concentrations of various species in premixed turbulent flames," Int. J. Hydrogen Energy **45**, 31162 (2020).
[15]A. N. Lipatnikov, V. A. Sabelnikov, F. E. Hernández-Pérez, W. Song, and H. G. Im, "A priori DNS study of applicability of flamelet concept to predicting mean concentrations of species in turbulent premixed flames at various Karlovitz numbers," Combust. Flame **222**, 370 (2020).
[16]A. N. Lipatnikov and V. A. Sabelnikov, "Evaluation of mean species mass fractions in premixed turbulent flames: A DNS study," Proc. Combust. Inst. **38**, 6413 (2021).
[17]A. N. Lipatnikov, V. A. Sabelnikov, F. E. Hernández-Pérez, W. Song, and H. G. Im, "Prediction of mean radical concentrations in lean hydrogen-air turbulent flames at different Karlovitz numbers adopting a newly extended flamelet-based presumed PDF," Combust. Flame **226**, 248 (2021).
[18]A. N. Lipatnikov, T. Nilsson, R. Yu, X.-S. Bai, and V. A. Sabelnikov, "Assessment of a flamelet approach to evaluating mean species mass fractions in moderately and highly turbulent premixed flames," Phys. Fluids **33**, 045121 (2021).
[19]H. C. Lee, P. Dai, M. Wan, and A. N Lipatnikov, "Influence of molecular transport on burning rate and conditioned species concentrations in highly turbulent premixed flames," J. Fluid Mech. **298**, A5 (2021).
[20]H. C. Lee, P. Dai, M. Wan, and A. N Lipatnikov, "Lewis number and preferential diffusion effects in lean hydrogen–air highly turbulent flames," Phys. Fluids **34**, 035131 (2022).
[21]M. Pfitzner, "A new analytic pdf for simulations of premixed turbulent combustion," Flow Turbul. Combust. **106**, 1213 (2021).
[22]M. Hansinger, M. Pfitzner and M. Klein, "Statistical analysis and verification of a new premixed combustion model with DNS data," Combust. Sci. Technol. **192,** 2093 (2020).
[23]M. Pfitzner and M. Klein, "A near-exact analytic solution of progress variable and pdf for single-step Arrhenius chemistry," Combust. Flame **226**, 380 (2021).
[24]M. Pfitzner and P. Breda, "An analytic probability density function for partially premixed flames with detailed chemistry," Phys. Fluids 33, 035117 (2021).
[25]M. Pfitzner, J. Shin, and M. Klein, "A multidimensional combustion model for oblique, wrinkled premixed flames," Combust. Flame **241**, 112121 (2022).
[26]T. Echekki, J. H. Chen, and I. Gran, "The mechanism of mutual annihilation of stoichiometric premixed methane-air flames," Proc. Combust. Inst. **26**, 855 (1996).
[27]J. H. Chen, T. Echekki, and W. Kollmann, "The mechanism of two dimensional pocket formation in lean premixed methane-air flames with implications to turbulent combustion," Combust. Flame **116**, 15 (1999).
[28]A. Y. Poludnenko and E. S. Oran, "The interaction of high-speed turbulence with flames: Turbulent flame speed," Combust. Flame **158**, 301 (2011).
[29]R. A. C. Griffiths, J. H. Chen, H. Kolla, and R. S. Cant, "Three-dimensional topology of turbulent premixed flame interaction," Proc. Combust. Inst. **35**, 1341 (2015).
[30]Y. Minamoto, K. Jigjid, R. Igari, and M. Tanahashi, "Effect of flame-flame interaction on scalar PDF in turbulent premixed flames," *Combust. Flame,* in press, https://doi.org/10.1016/j.combustflame.2021.111660
[31]H. L. Dave, A. Mohan, and S. Chaudhuri, "Genesis and evolution of premixed flames in turbulence," Combust. Flame **196**, 386 (2018).
[32]H. L. Dave and S. Chaudhuri, "Evolution of local flame displacement speeds in turbulence," J. Fluid Mech. **884**, A46 (2020).
[33]J. Li, Z. Zhao, A. Kazakov, and F. L. Dryer, "An updated comprehensive kinetic model of hydrogen combustion," Int. J. Chem. Kinetics **36**, 566 (2004).

[34]N. Babkovskaia, N. E. L. Haugen, A. Brandenburg, “A high-order public domain code for direct numerical simulations of turbulent combustion,” J. Comput. Phys. **230**, 1 (2011).

[35]T. J. Poinsot and S. K. Lele, “Boundary conditions for direct simulations of compressible viscous flows,” J. Comput. Phys. **101**, 104 (1992).

[36]V. A. Sabelnikov, R. Yu, and A. N. Lipatnikov, “Thin reaction zones in constant-density turbulent flows at low Damköhler numbers: Theory and simulations,” Phys. Fluids **31**, 055104 (2019).

[37]A. N. Lipatnikov and J. Chomiak, “Molecular transport effects on turbulent flame propagation and structure,” Prog. Energy Combust. Sci. **31**, 1 (2005).

[38]J. H. Chen and H. G. Im, “Stretch effects on the burning velocity of turbulent premixed hydrogen-air flames,” Proc. Combust. Inst. **28**, 211 (2000).

[39]H. G. Im and J. H. Chen, “Preferential diffusion effects on the burning rate of interacting turbulent premixed hydrogen-air flames,” Combust. Flame **131**, 246 (2002).

[40]V. A. Sabelnikov, A. N. Lipatnikov, S. Nishiki, H. L. Dave, F. E. Hernández-Pérez, W. Song, and H. G. Im, “Dissipation and dilatation rates in premixed turbulent flames,” Phys. Fluids **33**, 035112 (2021).